Design and Evaluation of Reduced-Rare-Earth Interior Consequent-pole Permanent Magnet Machines for Automotive Applications

Ya Li, *Member, IEEE*, Qinglin Zhou, Shichuan Ding, *Member, IEEE*, Wei Li, *Member, IEEE*, and Jun Hang, *Member, IEEE*

***Abstract*—This paper investigates the feasibility of interior consequent-pole permanent magnet (ICPM) machines with reduced rare-earth magnet consumption for automotive applications. A new ICPM machine with a double-layer V-shaped permanent magnet (PM) arrangement is proposed and compared with a commercial Nissan Leaf interior PM (IPM) machine. Their basic electromagnetic performances and rotor mechanical strength are evaluated by finite element (FE) simulation. It shows that the proposed ICPM machine exhibits comparable torque capability, similar high-efficiency region, and significantly improved PM utilization ratio compared with traditional Nissan Leaf IPM case. Besides, to verify the universality of ICPM designs with reduced-rare-earth consumption, two typical ICPM machines with different magnet configurations (single- and double-layer V-shaped) and power levels (80kW and 2kW) are respectively investigated and compared with their corresponding traditional IPM counterparts. Finally, some tested results on an ICPM machine prototype with V-shaped magnets are carried out to validate the FE analysis.**

***Index Terms*—Consequent-pole permanent magnet (PM), interior PM machine, reduced-rare-earth**

I. Introduction

DIFFERENT from conventional surfaced-mounted permanent magnet (SPM) machine, the N (or S) magnets are replaced by iron pole in consequent-pole permanent magnet (CPM) machine [1]. As a result, a unipolar permanent magnet (PM) magnetomotive force (MMF) distribution can be obtained in CPM machines [2]-[4]. In order to improve the rotor mechanical strength, the conventional surface-inset CPM concept is extended to the interior CPM (ICPM) machines with different PM arrangement in recent years.

Similar to traditional interior PM (IPM) machines, various ICPM machines with flat-type [5] [6], V-shaped [7]-[10], W-shaped [12], spoke-type [13]-[16], U-shaped [17]-[18] and ▽-shaped [19] PM structures are extensively developed and investigated. Compared with the conventional flat-type structure, the flat-type ICPM machine exhibits the same average torque and significantly reduced torque ripple by using the staggered rotor design [5]. Besides, the basic electromagnetic performances of SPM, CPM and ICPM machines with flat-type PM arrangement are evaluated in [6], which shows that a better demagnetization withstand capability compared with their SPM and CPM counterparts. Moreover, ICPM machine with V-shaped PM structure has a larger PM utilization ratio, lower torque ripple and cogging torque compared with conventional V-shaped IPM case [7]. In order to reduce flux leakage, a V-shaped ICPM machine with airspace flux barrier design is proposed in [8], the simulated and experimental results show a fact that the V-shaped structure has a great potential for applications in refrigerant compressor with relatively lower total cost due to its reduced PM usage. Besides, the ICPM machine with V-shaped PM arrangement exhibits greater power density and more abundant magnetic field harmonics for torque generation [9]. Because of the improved torque density with flux-enhancing effect and extended operation range in V-shaped structure, the ICPM machine exhibits more promising for variable speed application than SPM case [10]. A V-shaped ICPM vernier machine shows a prominent torque improvement and comparable efficiency compared with the benchmark of IPM counterpart due to its enhanced field modulation by stator teeth and hence resulting multiple working harmonics [11].

Besides, a W-shaped ICPM machine is presented in [12], the demagnetization withstand capability is estimated by finite element (FE) simulation, which shows that the higher demagnetization risk in high-speed operating range. Because of the flux-assisted design [13], the spoke-type ICPM configuration shows higher PM utilization ratio and wider constant power speed range than the conventional SPM counterpart. A spoke-type ICPM machine with asymmetrical modular PM design is investigated in [14]. It shows that a reduced flux leakage and improved field-weakening can be obtained [14]. In [15]-[16], an alternate flux barrier design is adopted in the spoke-type ICPM machine to improve low-order working harmonics. As a result, the low-order working field harmonic amplitudes and hence resulting enhanced torque capability can be obtained. Besides, a self-locking U-shaped PM design is employed in the ICPM machines to eliminate the iron bridges [17] [18], which exhibits higher PM utilization ratio and similar efficiency than the V-shaped counterparts [18]. Compared with the conventional cases, the ▽-shaped ICPM machine exhibits high torque and efficiency, lower cogging

This work was jointly supported in part by the National Natural Science Foundation of China (51607001, 52177027, 52107034), Excellent Youth Project of Natural Science Foundation of Anhui Province (2108085Y18), Key Project of Excellent Young Talents in University of Anhui Province (gxyqZD2021090) and Major science and technology special project of Anhui Province (202203c08020010). *(Corresponding author: Shichuan Ding)*

Ya Li, Qinglin Zhou, Shichuan Ding, Wei Li and Jun Hang are with the School of Electrical Engineering and Automation, Anhui University, Hefei 230601, P. R. China (e-mail: yali@ahu.edu.cn; z01814174@stu.ahu.edu.cn; dsc@ahu.edu.cn; liwei001x@163.com; hang_jun511@163.com).

torque, and better field-weakening capability [19].

Different from conventional ICPM arrangements, some new hybrid-pole ICPM machines are proposed by combining with surface-inset and interior magnet structures [20]-[24]. A hybrid-pole ICPM configuration with tangentially magnetized PMs is proposed to eliminate unipolar leakage flux in [20]. Moreover, the hybrid-pole ICPM structure shows similar torque capability, efficiency and slightly enhanced field-weakening capability compared with the SPM and surface-inset CPM designs [21]. Besides, the radial surface-inset and tangential spoke-type magnets are alternatively set in rotor to form a hybrid-pole ICPM machine [22]. The simulated results show that a relatively higher torque capability and PM utilization ratio can be achieved in those hybrid-pole ICPM machines compared with those conventional SPM and CPM topologies [23]-[24].

Although various ICPM machine with different PM arrangements are extensively developed and studied, the previous investigations are mainly focus on their performance evaluation and comparison. In order to estimate the feasibility of the rare-earth PM reduction in ICPM machine, a new double-layer V-shaped PM ICPM structure is proposed and compared with conventional Nissan Leaf IPM case in this paper. Besides, to verify the universality of PM consumption, two typical ICPM machines with different magnet configurations (double- and single-layer V-shaped) and power levels (80kW and 2kW) are respectively investigated and compared with the corresponding traditional IPM cases.

This paper is organized as follows. In Section II, the machine topology and is described. Then, the basic performances of the proposed ICPM machine is comprehensively investigated and compared with the and Nissan Leaf IPM machine in Section III. Furthermore, in Section IV, the influences of the PM arrangements and power levels on PM utilization ratio are evaluated. In Section V, an ICPM prototype with is manufactured, and some experimental measurements are carried out to verify the FE simulation, followed by the conclusion in Section VI.

II. Machine Topologies

An 8-pole/48-slot ICPM machine with double-layer V-shaped magnets is shown in Fig. 1(a). In order to validate the feasibility of the proposed design, the Nissan Leaf drive IPM machine is selected as the benchmark to perform a basic electromagnetic performance comparison, as illustrated in Fig. (b) [25]-[26]. It can be seen that the delta-type PM arrangement is adopted in Nissan Leaf IPM machine. The maximum torque and power of the Nissan Leaf IPM machine are 280Nm and 80kW, respectively [25]-[26]. To conduct a fair comparison, the two studied machines share the same stator structure, electrical load, axial length, and air-gap length. The corresponding key parameters of the two machines are tabulated in Table I.

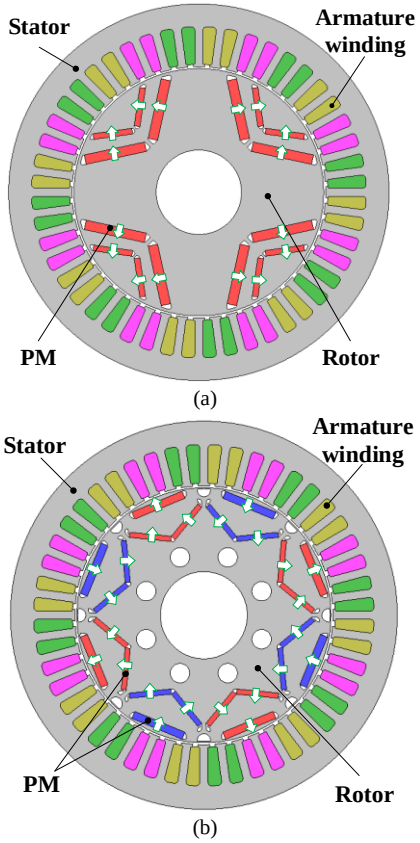

Fig. 1. Topologies of the 48-slot/8-pole ICPM and Nissan Leaf IPM machines. (a) ICPM machine. (b) Nissan Leaf IPM machine.

Table I
Main Design Parameters of the ICPM and Nissan Leaf IPM Machines

Parameters	ICPM	IPM
Stator slot number,	48	
Rotor poles,	8	
Stator outer radius, mm	99	
Active stack length, mm	151	
Stator inner radius, mm	66	
Air-gap length, mm	1.0	
Rotor outer radius, mm	65	
First-layer PM thickness, mm	4.5	3.8
First-layer PM length, mm	16.0	27.8
Second-layer PM thickness, mm	3.5	2.6
Second-layer PM length, mm	34.0	21.3
PM volume, cm^3	230.7	263.7
PM grade	N42UH	
Steel grade	B20AT1500	
Turns per phase	72	
Peak current, (A)	625	

To obtain a relatively better performance, a multi-objective genetic algorithm (GE) is adopted to optimize the average torque, PM volume and torque ripple of the proposed ICPM machine with the constraints of all the rotor design parameters. The flow-chart of the multi-objective GE is illustrated in Fig. 2. The objective functions are to maximize the average torque, and minimize PM volume and torque ripple. The optimized scatter diagram of the proposed ICPM machine is shown in Fig. 3. To balance the average torque, PM volume and torque ripple, the selected case is shown in Fig. 3, the corresponding main design parameters are listed in Table I.

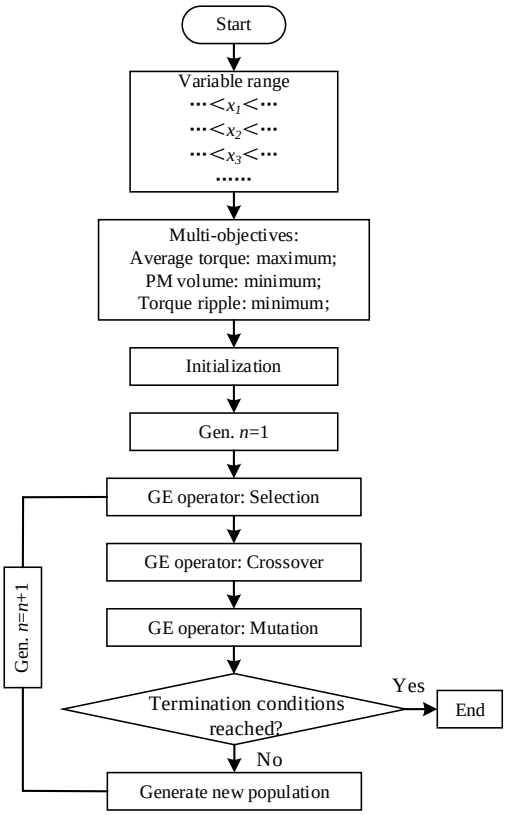

Fig. 2. The flow-chart of the multi-objective genetic algorithm.

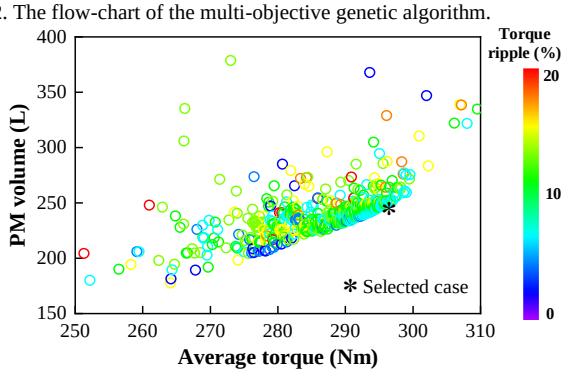

Fig. 3. Scatter diagram of the ICPM machine.

III. Performance Evaluation and Comparison

In order to confirm the feasibility of proposed ICPM machine with lower PM consumption, the basic electromagnetic and mechanical performances of the proposed and conventional Nissan Leaf IPM machines are evaluated and compared in this Section.

A. Open-Circuit Characteristics

The open-circuit magnetic field distributions of the two machines are shown in Fig. 4. Similar to the conventional Nissan Leaf IPM machine, the proposed ICPM design exhibits an 8-pole magnetic field distribution. The corresponding air-gap flux densities are given in Fig. 5. Different from the symmetrical air-gap flux density waveform in Nissan Leaf IPM machine, the ICPM machine exhibits an asymmetrical air-gap flux density waveform, which is mainly due to the unipolar PM MMF distribution. Besides, the proposed ICPM machine exhibits a relatively higher air-gap flux density fundamental harmonic amplitude than Nissan Leaf IPM configuration, which is mainly due to its reduced magnetic reluctance in ICPM machine. Consequently, a relatively higher PM utilization ratio can be obtained in proposed ICPM design. The open-circuit back-EMFs are shown in Fig. 6. It can be seen that the proposed ICPM design has an 8.4% higher fundamental harmonic amplitude than Nissan Leaf IPM machine. The total harmonic distortions (THDs) of the two machines are 12.2% and 8.9%, respectively. It implies that the proposed ICPM machine exhibits a relatively larger harmonic distribution and hence resulting a higher iron loss than Nissan Leaf IPM machine.

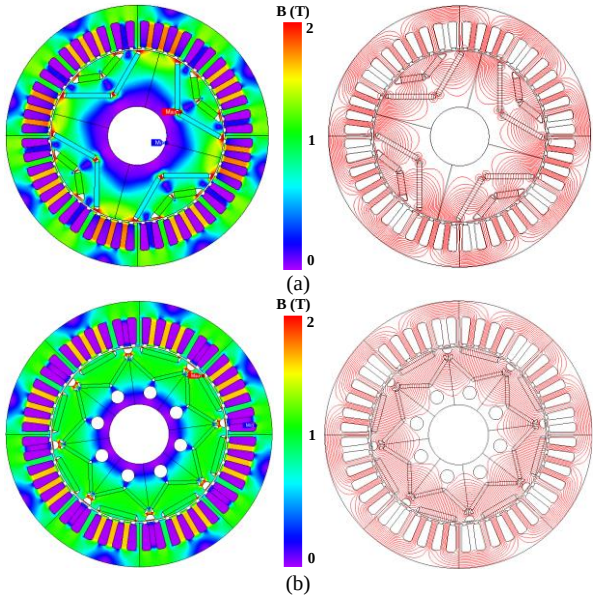

Fig. 4. Open-circuit magnetic flux distributions. (a) ICPM machine. (b) Nissan Leaf IPM machine.

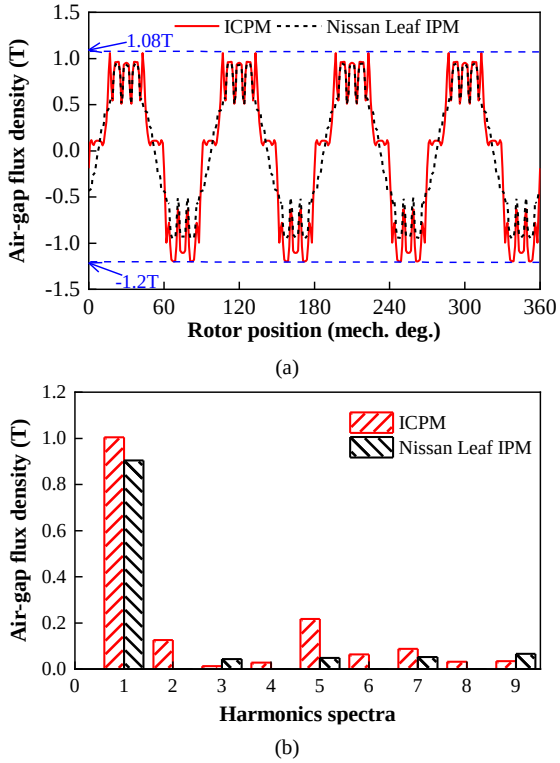

Fig. 5. Open-circuit air-gap flux density. (a) Waveforms. (b) Harmonics spectra.

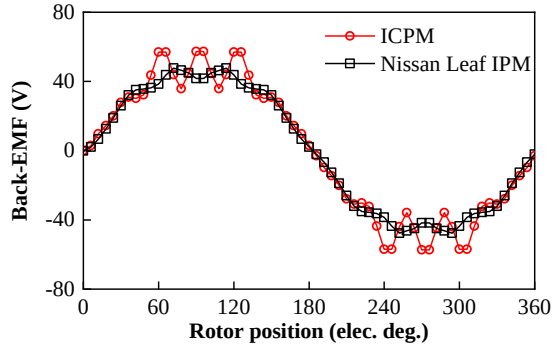

(a)

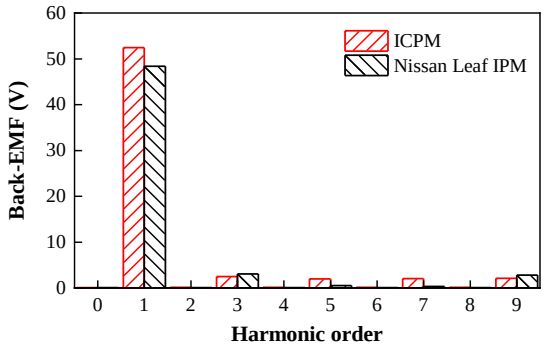

(b)

Fig. 6. Back-EMF @ 3000rpm. (a) Waveform. (b) Spectra.

B. *On-Load Torques*

The on-load torques of the two machines are shown in Fig. 7. It can be seen that the ICPM and Nissan Leaf IPM machines reach the maximum average torque values at 45 electrical degrees, and the maximum average torques are 293.1 Nm and 293.6 Nm, respectively. The reluctance torque and PM torque components of the two machines are shown in Fig. 7(b). Because of the reduced magnetic reluctance and improved air-gap flux density fundamental harmonic, the ICPM machine exhibits a relatively higher PM torque and lower reluctance torque than Nissan Leaf IPM case. The corresponding steady-state torque waveforms are plotted in Fig. 7(c). It indicates that the ICPM design with 10% reduced PM consumption exhibits comparable torque capability and hence higher PM utilization ratio than Nissan Leaf IPM machine.

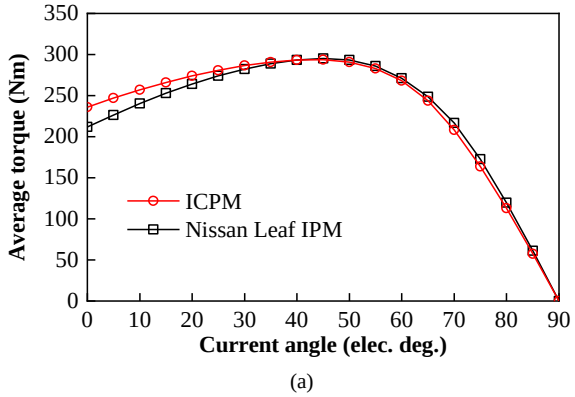

(a)

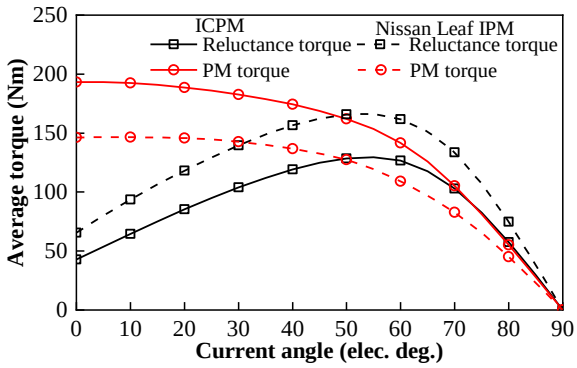

(b)

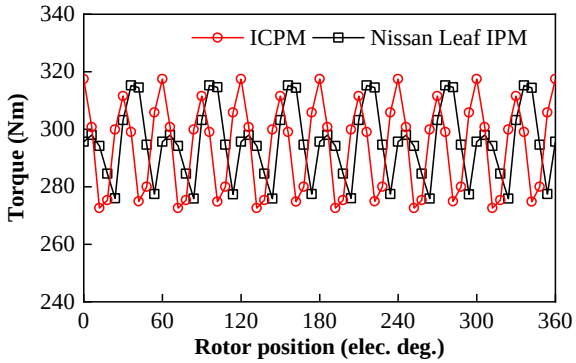

(c)

Fig. 7. On-load torques. (a) Average torque versus current angle curves. (b) Reluctance torque and PM torque components. (c) Steady-state torques.

C. *Torque/Power-Speed Curves*

The field-weakening factor can be defined as

$$k_{\mathrm{fw}} = \frac{L_{\mathrm{d}} I_{\max}}{\psi_{\mathrm{PM}}} \tag{1}$$

where L_{d} denotes d-axis inductance, $I_{\max}$ is the maximum phase current, ψ_{PM} is the PM flux linkage. Fig. 8 shows the torque and output power against speed curves. Compared with Nissan Leaf IPM machine, the proposed ICPM design exhibits a similar average torque and output power regardless speed, which is mainly due to the simultaneously reduced d-inductance and PM linkage in ICPM case. This indicates that a comparable field-weakening capability can be obtained in ICPM structure. The main electromagnetic parameters of the two machines are listed in Table II.

Table II
Main Electromagnetic Parameters of the ICPM and Nissan Leaf IPM Machines

Items	ICPM	Nissan Leaf IPM
L_{d}, (mH)	1.42	1.93
L_{q}, (mH)	3.01	3.03
$I_{\max}$, (A)	625	625
Ψ_{PM}, (Wb)	0.30	0.33
k_{fw}	1.35	1.31
Rotor iron loss, (W)	12.4	11.4
Stator iron loss (W)	240.0	219.5
PM eddy current loss (W)	16.2	14.3
Maximum efficiency (%)	97.1	97.2
High-efficiency region (%)	76.4	76.9

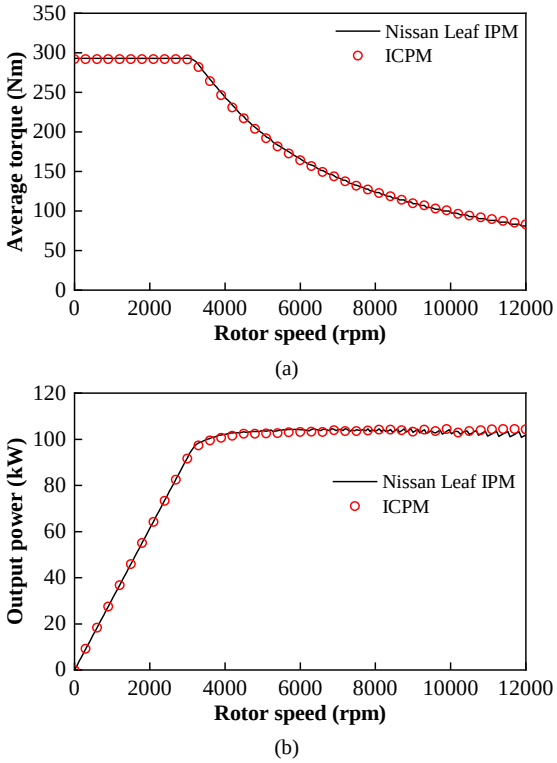

Fig. 8. Average torques/output power against rotor speed curves. (a) Average torques. (b) Output powers.

D. Demagnetization Withstand Capability

The B-H curves of the N42UH with different temperatures are given in Fig. 9. Because the maximum PM temperature rise in Nissan Leaf IPM machine is slightly lower than 100°C [27], the corresponding PM working temperature is set 100°C in the two machines to check the demagnetization risk. The reference knee point is approximately 0.06T at 100°C, as shown in Fig. 9. The demagnetization ratios [28] of the two machines at peak current condition are shown in Fig. 10. It can be seen that the minimal partial demagnetization occurs at the edges of PMs in the two machines. However, the maximum demagnetization ratios are very low and can be accepted, which confirms the two machines shows a good demagnetization withstand capability.

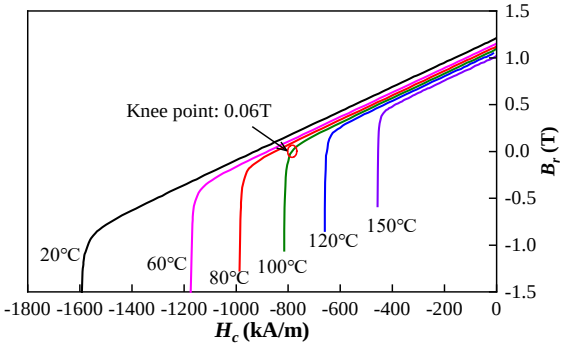

Fig. 9. B-H curves of the N42UH with different temperatures

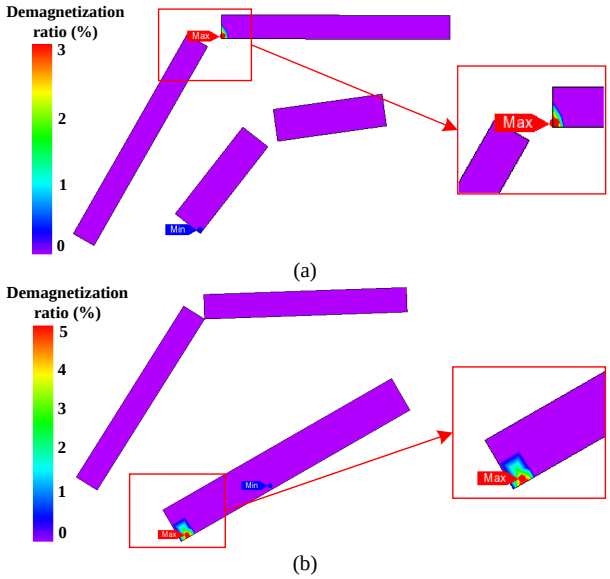

Fig. 10. Demagnetization ratios of the ICPM and Nissan Leaf IPM machines at peak current conditions. (a) ICPM machine. (b) Nissan Leaf IPM machine.

E. Loss and Efficiency Map

The iron loss distributions of the two machines under rated-load are shown in Fig. 11. It can be seen that the stator core has a relatively higher iron loss density than rotor core in the two machines. The iron loss and PM eddy-current loss against speed curves of the two machines are illustrated in Fig. 12(a) and (b), respectively. Compared with Nissan Leaf IPM machine, the proposed ICPM design exhibits a relatively higher iron and PM eddy-current losses regardless of speed, which is mainly due to the unipolar PM MMF distribution and hence resulting a more air-gap flux density harmonic. Taken the copper loss, iron loss and PM eddy current loss into consideration, the efficiency maps of the two machines are given in Fig. 13. The maximum efficiency of the ICPM and Nissan Leaf IPM machines are 97.1% and 97.2%, respectively. Their corresponding high-efficiency region (efficiency ≥ 90%) are 76.4% and 76.9%, respectively. This is mainly due to the slightly higher iron and PM eddy-current in ICPM design. However, the proposed ICPM machine exhibits a comparable efficiency distribution compared with traditional Nissan Leaf IPM case.

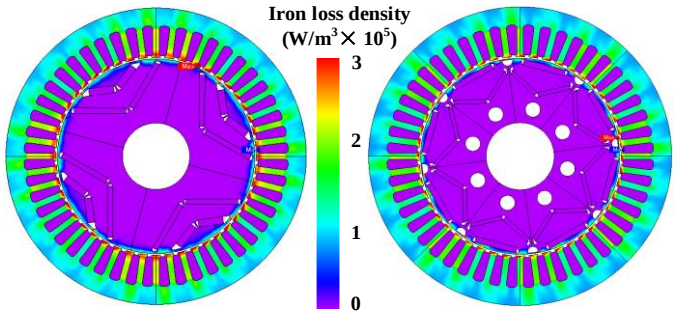

Fig. 11. Iron loss distributions of the ICPM and Nissan Leaf IPM machines under rated-load. (a) ICPM machine. (b) Nissan Leaf IPM machine.

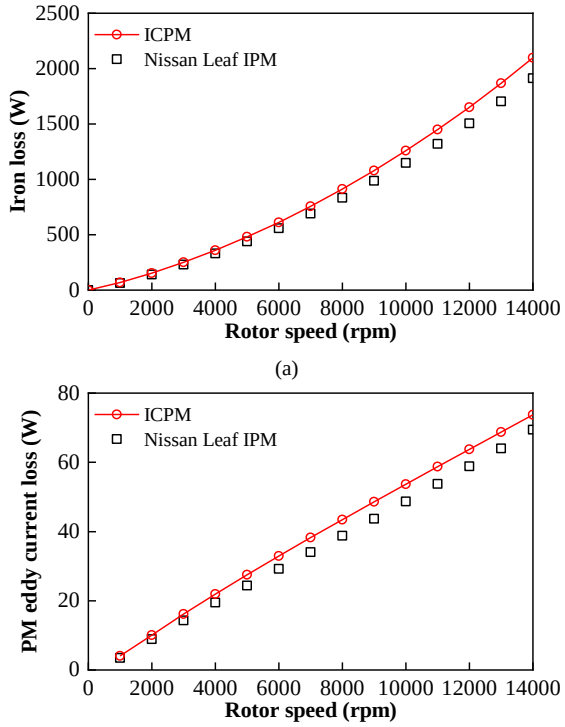

Fig. 12. Losses against rotor speed curves. (a) Iron loss. (b) PM eddy current loss.

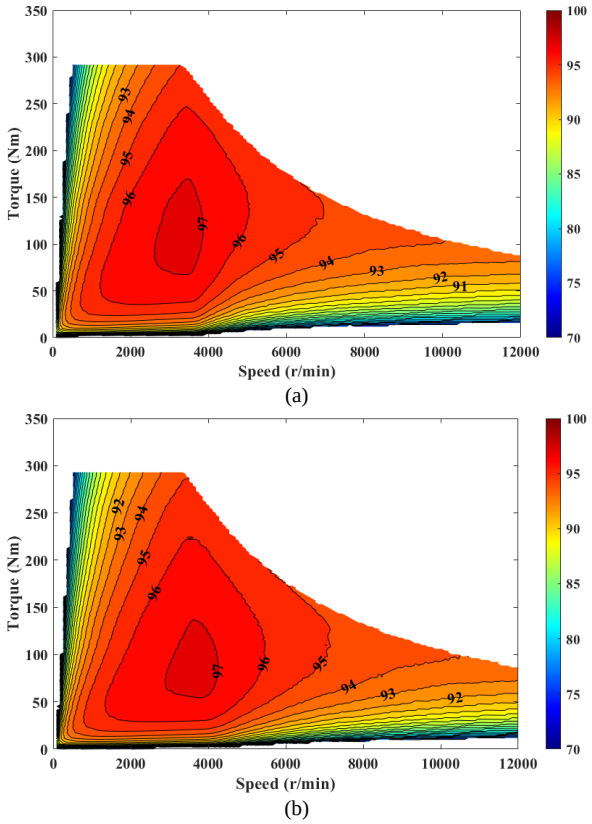

Fig. 13. Efficiency maps. (a) ICPM machine. (b) Nissan Leaf IPM machine.

F. Rotor Mechanical Strength

The Mise stress distributions of the two machines under peak speed condition are shown in Fig. 14. It can be found that the two rotor structures exhibit different stress distributions in rotor core due to their different PM arrangements. In addition, compared with Nissan Leaf IPM machine, the proposed ICPM design has a relatively lower value of the maximum Mises stress, which is attributed to its relatively lower PM consumption in per pole and hence resulting a slightly lower centrifugal force. The maximum stress values of the ICPM and Nissan Leaf IPM machines are 351.7 MPa and 360.8 MPa, which is less than the allowable yield strength of the 35CS250. Thus, proposed ICPM rotor structure can be satisfactorily addressed by adopting the iron bridges.

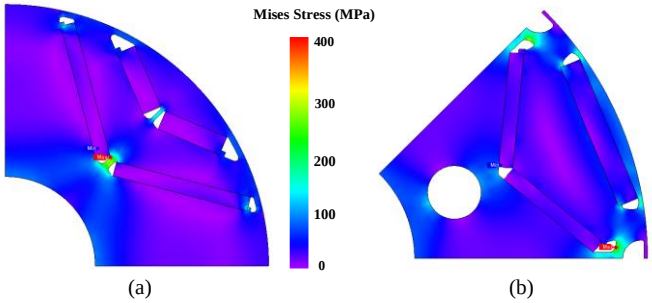

Fig. 14. Rotor mechanical stress distributions of the ICPM and Nissan Leaf IPM machines under peak speed (14000rpm). (a) ICPM. (b) Nissan Leaf IPM machine.

IV. Influences of PM Arrangements and Power Levels on PM Utilization Ratio

In order to confirm the feasible of the PM consumption reduction of the ICPM design, the influences of PM arrangement and power level on their basic electromagnetic are evaluated in this Section.

A. PM Arrangement

Fig. 15 shows the rotor structures of the traditional IPM and ICPM machines with single- and double-layer PM arrangements. The detailed parameters are listed in Tables III and IV. The air-gap flux densities of the four machines are illustrated in Figs. 16 and 17. Compared with traditional IPM machines, the ICPM designs with single- and double-layer PM configurations exhibit a comparable air-gap fundamental harmonic amplitude. Consequently, a similar torque capability can be obtained in ICPM machines. Besides, the ICPM machine with single- and double-layer PM structures have 22.3% and 16.3% reduced PM consumption compared with corresponding traditional IPM cases, respectively. It confirms the feasibility of the ICPM design for improving PM utilization. However, it should be noted that the PM reduction of double-layer V-shaped structure is slightly lower than corresponding single-layer case, which is mainly due to relatively serious PM flux leakage in iron bridges, as shown in Fig. 18.

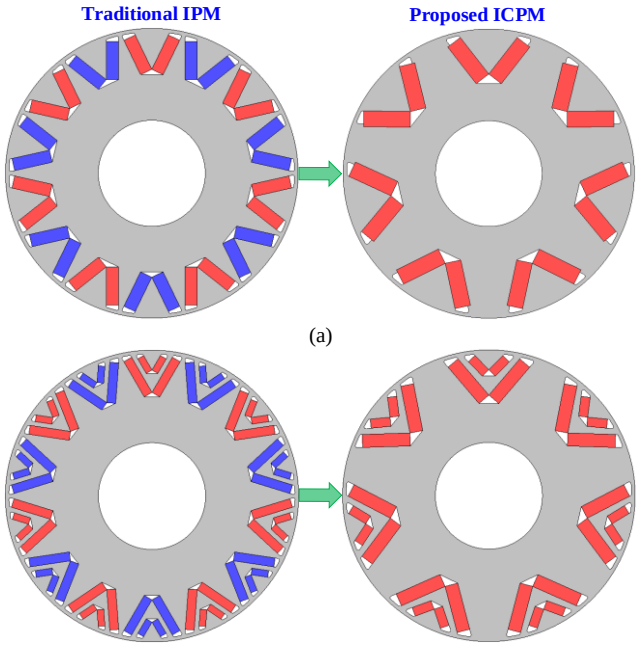

Fig. 15. Rotor structures of the traditional IPM machines and corresponding ICPM cases with different PM arrangements. (a) Single-layer V-shaped. (b) Double-layer V-shaped.

Table III
Main design parameters of the traditional IPM and ICPM machines with Single-layer V-shaped PM arrangement

Items	IPM and ICPM machines			
PM structure	IPM	ICPM	IPM	ICPM
Power levels, (kW)	2		80	
Stator-slot/rotor-pole	12/14		48/8	
Stator outer radius, (mm)	61		100	
Stator inner radius, (mm)	33.3		66	
Air-gap length, (mm)	0.5		1.0	
Axial length, (mm)	55		151	
Average torque, (Nm)	19.1	19.2	294.5	293.9
PM volume, (cm3)	37.2	28.9	298.8	265.4
Torque/PM volume, (Nm/L)	513.4	**634.6**	985.5	1107.4
PM reduction %	/	**22.3**	/	**11.2**

Table IV
Main design parameters of the traditional IPM and ICPM machines with Double-layer V-shaped PM arrangement

Items	IPM and ICPM machines			
PM structure	IPM	ICPM	IPM	ICPM
Power levels, (kW)	2		80	
Stator-slot/rotor-pole	12/14		48/8	
Stator outer radius, (mm)	61		100	
Stator inner radius, (mm)	33.3		66	
Air-gap length, (mm)	0.5		1.0	
Axial length, (mm)	55		151	
Average torque, (Nm)	18.4	18.2	295.7	293.5
PM volume, (cm3)	36.8	30.8	287.8	241.6
Torque/PM volume, (Nm/L)	447.9	**590.9**	1027.4	1214.8
PM reduction %	/	**16.3**	/	**12.6**

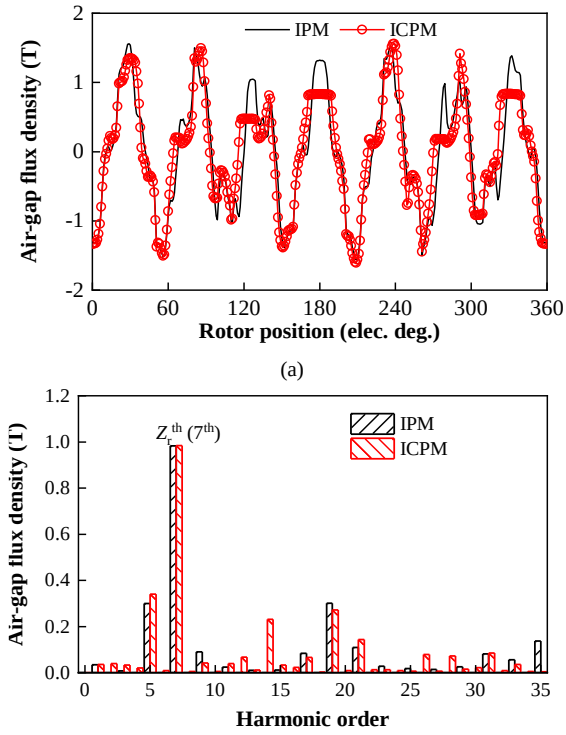

Fig. 16. Air-gap flux density of the traditional IPM and ICPM machines with single-layer V-shaped PM arrangement. (a) Waveforms. (b) Spectra.

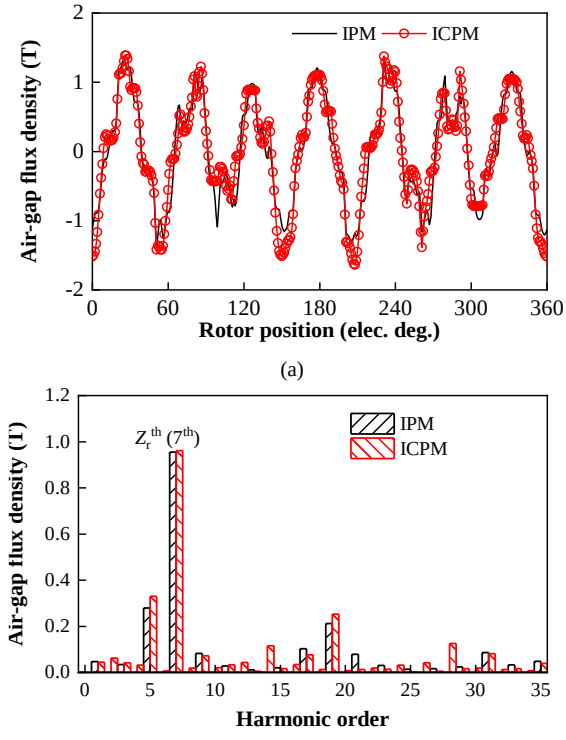

Fig. 17. Air-gap flux density of the traditional IPM and ICPM machines with double V-shaped PM arrangement. (a) Waveforms. (b) Spectra.

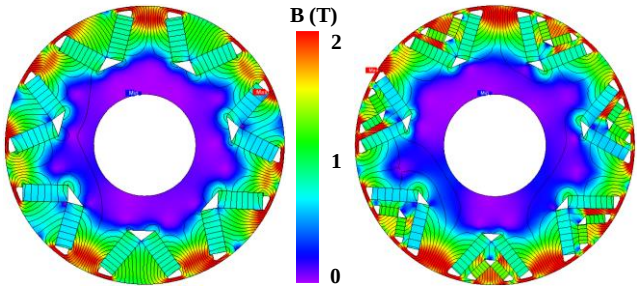

(a) (b)

Fig. 18. Flux density distributions of the ICPM machines with single- and double-layer V-shaped PM arrangements. (a) Single-layer. (b) Double-layer.

B. *Power Levels*

The main parameters of the single- and double-layer V-shaped magnet ICPM machines with 2kW and 80kW power levels are shown in Tables III and IV. Compared with conventional IPM machines, the proposed ICPM designs exhibit a relatively lower PM consumption, which confirms a feasibility of PM reduction of the ICPM design regardless of power levels. It can be found that the 80kW ICPM machine with double-layer V-shaped PM structure exhibits a relatively higher PM reduction compared with corresponding single-layer V-shaped case, which is mainly due to the improved reluctance torque in double-layer V-shaped arrangement.

In order to quantify the axial magnetic leakage, the difference of 2D and 3D simulated average torques can be expressed as

$$\Delta T = \frac{T_{2D} - T_{3D}}{T_{2D}} \times 100\% \quad (2)$$

where T_{2D} and T_{3D} are the 2D and 3D simulated average torque values, respectively. The differences of the ICPM machines with 2kW and 80kW are plotted in Fig. 19. Compared with 2kW ICPM machines, the 80kW ICPM structures exhibit a relatively lower axial magnetic leakage, as shown in Fig. 20.

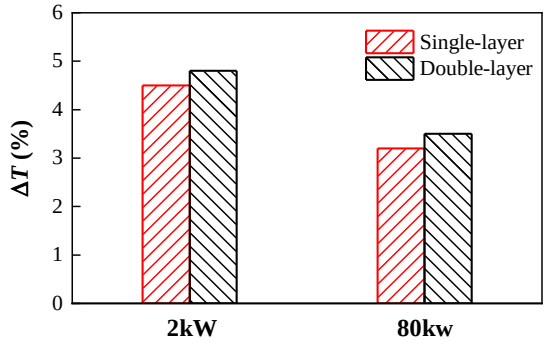

Fig. 19. Difference of 2D and 3D simulated average torque values of the 2kW and 80kW ICPM machines with single- and double-layer V-shaped magnets.

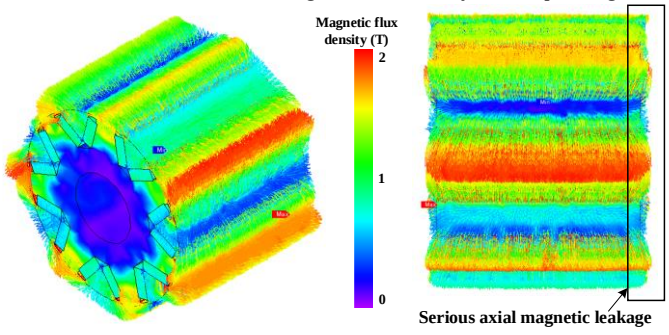

(a)

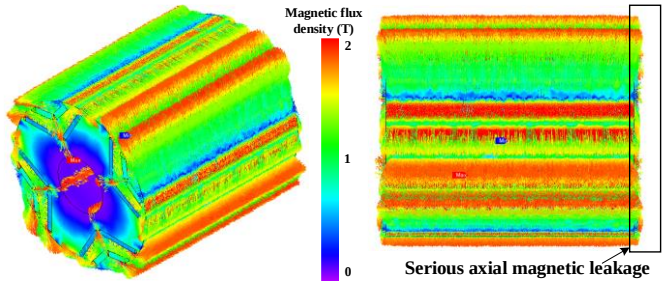

(b)

Fig. 20. Magnetic field distributions of the ICPM machines with single- and double-layer V-shaped PM arrangements at peak-current load. (a) Single-layer (2kW). (b) Double-layer (80kW).

V. Experimental Validation

In order to experimentally validate FE simulation, an optimized12-slot/14-pole ICPM machine prototype with V-shaped PM structure is manufactured. Some tested results on the prototype are conducted. The pictures of the stator and rotor assemblies are given in Figs. 21 (a) and (b), respectively. The test-rig is illustrated in Fig. 21(c).

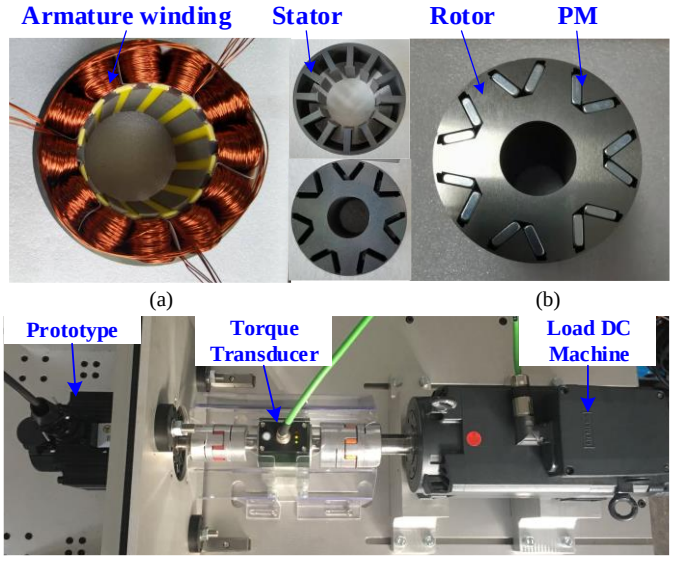

(a) (b)

(c)

Fig. 21. ICPM machine prototype and test-rig. (a) Stator. (b) Rotor. (c) Test-rig.

A. *No-load Back-EMF*

The no-load back-EMF of the machine prototype under rated speed 1000rpm can be measured by the test-rig when the load DC-machine operating at motoring condition. The corresponding tested, 2D and 3D FE simulated back-EMF waveforms and their harmonic spectra are plotted in Fig. 22. It can be observed that the measured back-EMF waveform matches well with 2D and3D FE results, as shown in Fig. 22(a), which confirms that the effectiveness of FE simulation. However, the tested back-EMF fundamental harmonic amplitude is slightly lower than the 2D and 3D FE simulated values, which is mainly due to the mismatching tolerance in prototype. Besides, because the end-winding effect and axial magnetic leakage are taken into consideration of the 3D FE simulation, the 3D predictions are closer to the tested values than 2D FE simulation.

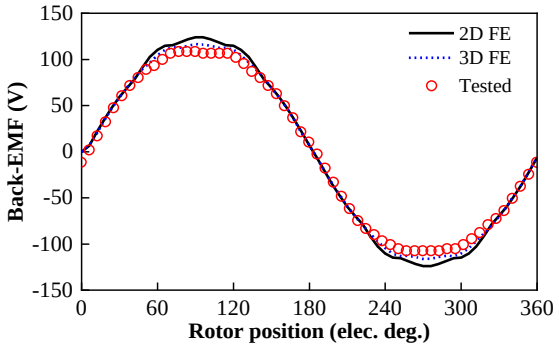

(a)

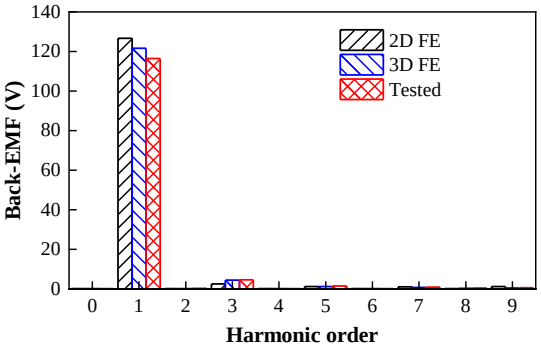

(b)

Fig. 22. Comparison of FE predicted and measured open-circuit back-EMFs of the prototype. (a) Waveforms. (b) Harmonic spectra.

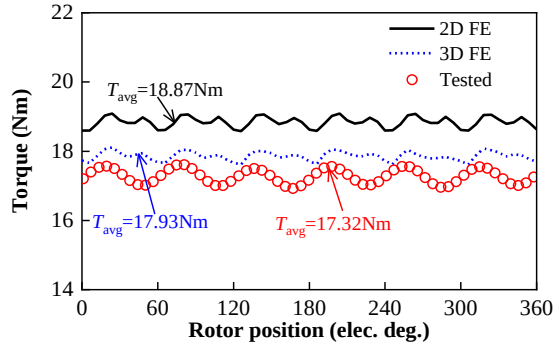

(a)

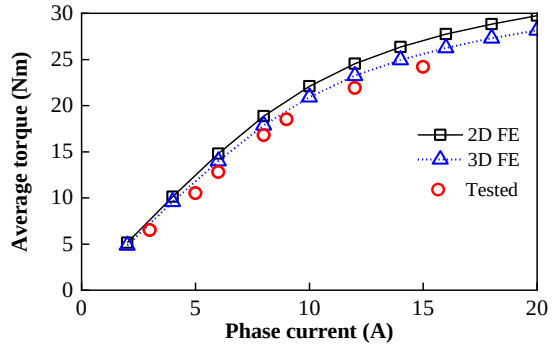

(b)

Fig. 23. Tested and FE simulated torques. (a) Steady-state torque waveforms at rated-load condition. (b) Average torques against phase current.

B. On-load Torque

When the load DC machine is used to generate a load torque for the tested prototype, the dynamic torque can be measured via torque transducer. Because of the reluctance torque is very low and can be neglected in fractional-slot concentrated winding, the i_d=0 control is adopted in this prototype experiment. Fig. 23(a) shows the tested, 2D and 3D FE simulated steady torque waveforms of the prototype operating at rated-load condition. It can be seen that the measured steady-torque waveform agrees well with the simulation results. The tested average torques with different phase currents are compared with 2D and 3D FE simulations, as shown in Fig. 23(b). Similarly, the measured average torques match well with 2D and 3D FE predictions regardless of the phase currents. However, because of the neglected manufactured tolerance in prototype, the tested torques are slightly lower that 2D and 3D FE simulations. In addition, the mismatch of the measured and FE simulated slightly increased with phase current due to the serious axial flux leakage in overload condition. Overall, a good agreement between the tested and FE simulations verifies the effectiveness of the abovementioned analyses.

VI. Conclusions

This paper investigates the feasibility of the PM reduction in ICPM machine for automotive applications. A new ICPM machine with double-layer V-shaped PM arrangement is proposed and evaluated. The basic performances of the proposed ICPM and conventional Nissan Leaf IPM machines are investigated and compared. It shows that the proposed ICPM machine exhibits a comparable torque capability, field-weakening ability, similar lower high-efficiency region and significantly reduced PM consumption compared with Nissan Leaf IPM case. Additionally, the influences of PM structure and power level on the feasibility of ICPM machines are estimated and compared with corresponding IPM cases. It confirms a fact that the 2kW and 80kW ICPM machines exhibit a relatively larger PM reduction in single- and double-layer PM structures, respectively. Lastly, an ICPM machine prototype is manufactured and some tested results validate the FE simulation.

References

[1] J. A. Tapia, F. Leonardi and T. A. Lipo, "Consequent-pole permanent-magnet machine with extended field-weakening capability," *IEEE Trans. Ind. Appl*., vol. 39, no. 6, pp. 1704-1709, Nov. /Dec. 2003.

[2] Y. Li, H. Yang, H. Lin, L. Qin, and S. Lyu, "Investigation of double-side field modulation mechanism in consequent-pole PM machines with concentrated windings," *IEEE Trans. Energy Convers*., vol. 36, no. 3, pp. 1635-1648, Sep. 2021.

[3] S. U. Chung, J. W. Kim, Y. D. Chun, B. C. Woo and D. K. Hong, "Fractional slot concentrated winding PMSM with consequent pole rotor for a low-speed direct drive: reduction of rare earth permanent magnet," *IEEE Trans. Energy Convers*., vol. 30, no. 1, pp. 103-109, Mar. 2015.

[4] H. Dhulipati, E. Ghosh, S. Mukundan, P. Korta, J. Tjong and N. C. Kar, "Advanced design optimization technique for torque profile improvement in six-phase PMSM using supervised machine learning for direct-drive EV," *IEEE Trans. Energy Convers*., vol. 34, no. 4, pp. 2041-2051, Dec. 2019.

[5] T. Watahiki, Y. Toriumi and I. Miki, "A consequent pole motor with novel pole structure," in *Proc. Int. Symp. Power Electronic, Elec. Drive, Auto. Motion*, 2018, pp. 1136-1140.

[6] R. Zhou, G. J. Li, Z. Q. Zhu, Y. X. Li, M. P. Foster and D. A. Stone, "Investigation of integer/fractional slot consequent pole PM machines with different rotor structures," in *Proc. 2019 IEEE Int. Elec. Mach. Drive Conf. (ICEMS)*, 2019, pp. 119-126.

[7] L. Wu and R. Qu, "Comparison of conventional and consequent pole interior permanent magnet machines for electric vehicle application," in *Proc. 17th Int. Conf. Elec. Mach. & Sys. (ICEMS)*, 2014, pp. 70-74.

[8] M. T. Chiu, J. A. Chiang and C. H. Lin, "Design and optimization of a novel V-type consequent-pole interior permanent magnet synchronous motor for applying to refrigerant compressor," in *Proc. 21st Int. Conf. Electri. Sys. (ICEMS)*, 2018, pp. 413-418.

[9] G. Qu, Y. Fan and R. Cui, "Design and analysis of a new consequent-pole interior permanent magnet synchronous motor," in *Proc. 21st Int. Conf. Electri. Sys. (ICEMS)*, 2018, pp. 376-381.

[10] S. Cai, Z. Q. Zhu, S. Mallampalli, J. C. Mipo and S. Personnaz, "Investigation of novel fractional slot nonoverlapping winding hybrid excited machines with different rotor topologies," *IEEE Trans. Ind. Appl.*, vol. 57, no. 1, pp. 468-480, Jan. /Feb. 2021.

[11] W. Liu, J. Wang, and T. A. Lipo, "A consequent pole single rotor single stator vernier design to effectively improve torque density of an industrial PM drive," *IEEE Trans. Ind. Electron.*, accepted, 2022, doi: 10.1109/TIE.2022.3153806.

[12] R. E. Q. Palomo and M. Gwozdziewicz, "Effect of demagnetization on a consequent pole IPM synchronous generator," *Energies*, vol. 13, no. 6371, pp. 1-13, Dec. 2020.

[13] M. Onsal, B. Cumhur, Y. Demir, E. Yolacan and M. Aydin, "Rotor design optimization of a new flux-assisted consequent pole spoke-type permanent magnet torque motor for low-speed applications," *IEEE Trans. Magn.*, vol. 54, no. 11, Nov. 2018, Art. no. 8206005.

[14] J. Li and K. Wang, "A novel spoke-type PM machine employing asymmetric modular consequent-pole rotor," *IEEE/ASME Trans. Mech.*, vol. 24, no. 5, pp. 2182-2192, Oct. 2019.

[15] W. Liu and T. A. Lipo, "Analysis of consequent pole spoke type vernier permanent magnet machine with alternating flux barrier design," *IEEE Trans. Ind. Appl.*, vol. 54, no. 6, pp. 5918-5929, Nov. /Dec. 2018.

[16] X. Ren, D. Li, R. Qu, Z. Yu, and Y. Gao, "Investigation of spoke array permanent magnet vernier machine with alternate flux bridges," *IEEE Energy Convers.*, vol. 33, no. 4, pp. 2112-2121, Dec. 2018.

[17] J. Kolehmainen, "Optimal dovetail permanent magnet rotor solutions for various pole numbers," *IEEE Trans. Ind. Electron.*, vol. 57, no. 1, pp. 70-77, Jan. 2010.

[18] J. Li, K. Wang and H. Zhang, "Flux-focusing permanent magnet machines with modular consequent-pole rotor," *IEEE Trans. Ind. Electron.*, vol. 67, no. 5, pp. 3374-3385, May 2020.

[19] L. Zhang, K. Wang, J. Li and F. Li, "Comparison study of interior permanent magnet synchronous machine with conventional and consequent pole rotor," in *Proc. 22st Int. Conf. Electri. Sys. (ICEMS)*, 2019, pp. 1-5.

[20] K. Wang, J. Li, S. S. Zhu and C. Liu, "Novel hybrid-pole rotors for consequent-pole PM machines without unipolar leakage flux," *IEEE Trans. Ind. Electron.*, vol. 66, no. 9, pp. 6811-6823, Sep. 2019.

[21] J. Li, K. Wang and C. Liu, "Comparative study of consequent-pole and hybrid-pole permanent magnet machines," *IEEE Trans. Energy Convers.*, vol. 34, no. 2, pp. 701-711, Jun. 2019.

[22] G. Dajaku, "Open circuit air-gap field calculation of a new PM machine having a combined SPM and spoke type magnets," *IEEE Trans. Magn.*, vol. 56, no. 6, Jun. 2020, Art. no. 8200409.

[23] G. Dajaku, "Comparison study of permanent magnet synchronous machines with consequent pole and HUPM rotor," *IEEE Trans. Magn.*, vol. 58, no. 3, Mar. 2022, Art. no. 8104110.

[24] G. Xu, W. Zhao, G. Liu, F. Zhai and Q. Chen, "Torque performance improvement of consequent-pole PM motors with hybrid rotor configuration," *IEEE Trans. Transport. Electrific.*, vol. 7, no. 3, pp.1561-1572, Sep. 2021.

[25] Y. Sato, S. Ishikawa, T. Okubo, M. Abe, and K. Tamai, "Development of high response motor and inverter system for the Nissan Leaf electric vehicle," *SAE International*, vol. 1, no. 342, pp. 104-111, 2011.

[26] T. Burress, "Benchmarking of competitive technologies," Oak Ridge National Laboratory, 2012, [Online]. Available: http://www1.eere.energy.gov/vehiclesandfuels/pdfs/merit_review_2012/adv_power_electronics'/ape006_burress_2012.p.pdf, Dec. 2015.

[27] G. Moreno, "Thermal performance benchmarking: annual report," National Renewable Energy Laboratory (NREL), Apr. 2016.

[28] Y. Yang, S. M. Castano, R. Yang, M. Kasprzak, B. Bilgin, A. Sathyan, H. Dadkhah, and A. Emadi, "Design and comparison of interior permanent magnet motor topologies for traction applications," *IEEE Trans. Transport. Electrific.*, vol. 3, no. 1, pp. 86-97, Mar. 2017.

Ya Li (Member, IEEE) received the B. Eng. Degree in School of Electronic and Electrical Engineering from Shangqiu Normal University, Shangqiu, China, in 2014, and the M. S. Degree in School of Electrical Engineering and Automation from Jiangxi University of Science and Technology, Jiangxi, China, in 2017, and the Ph.D. degree in degree in School of Electrical Engineering from Southeast University, Nanjing, in 2021.

Since 2022, he has been with Anhui University, Hefei, China, where he is currently a Lecturer. His research interests include design, and analysis of the permanent magnet machines.

Qinglin Zhou received the B. Eng. Degree in School of Electrical Engineering and Automation from Anhui University, Hefei, China, in 2022, She is currently working toward the Ph. D. degree in School of Electrical Engineering and Automation at Anhui University, Hefei, China.

Her current research interests design, and analysis of the synchronous machines.

Shichuan Ding (S'08-M'12) received the B.Sc. degree in automation from Anhui University, Hefei, China, in 2001 and the M.Sc. degree from University of Science and Technology of China, Hefei, China, in 2006, and the Ph.D. degree in electrical engineering from Southeast University, Nanjing, China, in 2018.

Since 2001, he has been with Anhui University, where he is currently a Professor. He has been a Research Scholar with WEMPEC in University of Wisconsin Madison from April 2015 to April 2016. His research interests include electrical machine drive, power electronics applications and energy management in EVs and in power system. In recent years, he has authored and co-authored over 30 technical papers.

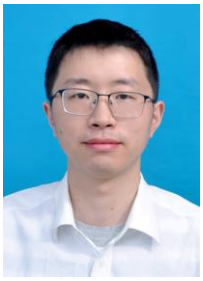

Wei Li (Member, IEEE) received the B.Sc. degree from Anhui University of Technology, Ma'anshan, China, in 2008, the M.E. degree from Anhui University, Hefei, China, in 2012, and the Ph.D degrees from the School of Electrical Engineering, Southeast University, Nanjing, China, in 2019. Since 2017, he has been with Anhui University, Hefei, China. His current research interests include the reliability of permanent magnet machines for application in hybrid vehicles.

Jun Hang (S'12-M'16) received the B.Sc. and M.Sc. degrees in Electrical Engineering from Anhui University of Science & Technology, Huainan, China, in 2008 and 2011, respectively, and the Ph.D. degree in electrical engineering from Southeast University, Nanjing, China, in 2016. From April 2015 to July 2015, He was a joint Ph. D. student with the Department of Energy Technology, Aalborg University, Denmark.

Since 2016, he has been with Anhui University, Hefei, China, where he is currently an Associate Professor in the School of Electrical Engineering and Automation. His current research interests include condition monitoring, fault diagnosis, permanent magnet machine and renewable energy. In recent years, he has authored and co-authored over 30 technical papers.

Dr. Hang received the 1st Prize of 2016 Student Thesis Contest (PhD Category), IEEE Industry Applications Society.